Modeling the microbial contribution to human Energy Balance using the Digestion, Absorption, and Microbial Metabolism (DAMM) model

Taylor L. Davis[1,2], Blake Dirks[1,2], Elvis A. Carnero[3], Karen D. Corbin[4], Steven R. Smith[4], Andrew Marcus[4], Rosa Krajmalnik-Brown[1,5], and Bruce E Rittmann[2,5]

Abstract

Colonic microorganisms have been linked to human health and disease, specifically metabolic disease states such as obesity, but causal relationships remain to be established. Previous work demonstrated that interactions between the host's diet and intestinal microbiome were associated with human energy balance by affecting the human's energy absorption, quantified by metabolizable energy. We developed the Digestion, Absorption and Microbial Metabolism (DAMM) model, which explicitly accounts for the energy contributions of the colonic microbial community by: 1) breaking down the diet composition into the gross energy of the individual macronutrients, 2) calculating direct absorption in the upper gastrointestinal tract, 3) using microbial stoichiometry to estimate the consumption of the remaining unabsorbed nutrients by microbes in the large intestine, and 4) quantifying predicted production of microbial products (short-chain fatty acids (SCFA) and methane) in the colon and estimating absorption from the colonic tract to the host. When used to predict the results from a clinical study that compared two distinctly different diets, the DAMM model captured the directionality and magnitude of change in measured metabolizable chemical oxygen demand (which can be converted to metabolizable

[1] Biodesign Center for Health through Microbiomes, Arizona State University, Tempe, AZ, USA.
[2] Biodesign Swette Center for Environmental Biotechnology, Arizona State University, Tempe, AZ, USA.
[3] AdventHealth Translational Research Institute, Orlando, FL, USA.
[4] Great Lakes Water Authority, Detroit, MI, USA.
[5] School of Sustainable Engineering and the Built Environment, Arizona State University, Tempe, AZ, USA.

energy), improved on the accuracy of predictions compared to the Atwater factors by reducing systematic bias on one of the diets, and estimated substrate availability within the colon and rate of production of microbially derived short-chain fatty acids. Measured methane concentrations, combined with findings from the DAMM model, support the hypothesis that methanogens accumulated in mucosal biofilms in participants harboring methanogens. Model outputs also support that colonic transit time directly influenced SCFA absorption rates. The DAMM model now can be linked to existing human models that predict changes in body energy stores to extend our understanding of how microbial metabolic processes affect macronutrient absorption and metabolizable energy.

Keywords

human macronutrient digestion and metabolism, microbial short-chain fatty acid metabolism, mathematical model, methanogenesis, gut microbiome

Acronym Table

Acronym/Variable	*Name*	*Unit*	*Description*
amt_{food}	Mass of consumed food item per day	g_{food} d^{-1}	The amount of a food item consumed in a day
COD	Chemical oxygen demand	gCOD	An indicative measure of the amount of oxygen that can be consumed, directly proportional to the electron equivalents in a food's carbon.
$COD_{biomass}$	Specific chemical oxygen demand for biomass	gCOD $g_{biomass}^{-1}$	COD per gram for a biomass for $C_5H_7O_2N$
COD_{CH4}	Methane chemical oxygen demand	gCOD d^{-1}	Daily COD that leaves the human body as methane gas.
COD_f	Fecal chemical oxygen demand	gCOD d^{-1}	Total daily amount of ingested COD that is expelled in the feces (can be specified as only from specific nutrient N)
COD_g	Gross chemical oxygen demand	gCOD d^{-1}	Total daily amount of ingested COD from food (can be specific to a nutrient i.e. COD_g^{starch} would be the total ingested COD of starch)
COD_m	Metabolizable chemical oxygen demand	gCOD d^{-1}	Total daily amount of ingested COD that is metabolizable by the host (can be specified as only from UGI or LGI or a specific nutrient N)
$COD_{nutrient}$	Specific chemical oxygen demand of nutrient	gCOD $g_{nutrient}^{-1}$	COD per gram for a specific nutrient calculated using chemical formula
CSTR	Continuously stirred reactor		A tank reactor characterized by a continuous flow of reactants into and products from the reaction system
CTT	Colonic transit time	d	Time duration it takes for ingested food to travel from the ileocecal valve to the anus
DAMM	Digestion, Absorption, and Microbial Metabolism		Mathematical model that tracks the progression of ingested macronutrients as they advance through the host's digestive tract until they are subsequently absorbed and metabolized by organs and tissues or excreted – includes microbial contributions explicitly

E_g	Gross energy	kcal d^{-1}	Total combustible energy within food items of a diet, usually expressed as a rate
E_m	Metabolizable energy	kcal d^{-1}	Amount of energy available for human metabolic processes after absorption in the digestive tract, usually expressed as a rate
$e_{scfa\ abs}$	Efficiency of SCFA absorption	$gCOD_{abs}\ gCOD^{-1}$	Proportion of SCFAs that are absorbed within the colon calculated using saturation model dependent on CTT
f_{dry}	Fraction of dry mass	$g_{dry\ wt}\ g_{wet\ wt}^{-1}$	Mass fraction of dry mass to wet mass
$f_{nutrient}$	Mass fraction of nutrient in food item	$g_{nutrient}\ g_{food}^{-1}$	The amount of a specific nutrient in a food item (e.g. the fraction of starch in potatoes)
f_{org}	Fraction of organic dry mass	$g_{org\ dry\ wt}\ g_{dry\ wt}^{-1}$	Mass fraction of organic dry mass to dry mass
$k_{C\ ferm}$	Carbohydrate fermentation coefficient	$gCOD^{-1}\ d^{-1}$	Second-order kinetic coefficient for fermentation of simple sugars like glucose or fructose
$k_{C\ hyd}$	Carbohydrate hydrolysis coefficient	$gCOD^{-1}\ d^{-1}$	Second-order kinetic coefficient for hydrolysis of complex carbohydrates like fiber or resistant starch
$k_{F\ abs}$	Fat absorption coefficient	d^{-1}	First-order absorption coefficient for fat in the LGI
k_M	Methanogenesis coefficient	$gCOD^{-1}\ d^{-1}$	Second-order kinetic coefficient for methanogenesis
$k_{P\ hyd}$	Protein hydrolysis coefficient	$gCOD^{-1}\ d^{-1}$	Second-order kinetic coefficient for hydrolysis of proteins into amino acids
$K_{scfa\ abs}$	Half-saturation constant for SCFA abosrption	d	Half-saturation constant for absorption of SCFAs in the LGI
LGI	Lower gastrointestinal tract		Subsection of the gastrointestinal tract encompassing the passageway from the start of the colon to the anus
MBD	Microbial enhancer diet		One of two diets within the clinical trial with the same ratios of carbohydrates, proteins, and fats and the necessary calories to remain in energy balance, this diet was designed to increase the available substrates for the gut microbes
mcrA	Methyl coenzyme M reductase	copy #	Enzyme that catalyzes the final step in the formation of methane, also known as coenzyme-B sulfoethylthiotransferase

N	Nutrient	gCOD	A specific nutrient considered within the diet (e.g. starch, glucose, alanine, DHA, etc.)
N_{copy}	Gene copy number per cell	copy # $cell^{-1}$	Typical number of copies for a specific gene (*mcrA* in this work) within a cell
qPCR	Quantitative polymerase chain reaction		Laboratory technology used for measuring DNA using polymerase chain reaction.
R^2	Coefficient of determination		Measure of how well observed outcomes are replicated by the model
R_{ut}	Utilization rate per day	gCOD d^{-1}	Total utilization rate per day – included five processes: 1) protein hydrolysis and fermentation 2) carbohydrate hydrolysis and fermentation 3) methanogenesis 4) absorption of fat in colon and 5) absorption of SCFAs in colon
SCFA	Short-chain fatty acids		Fatty acids of two to four carbon atoms. In this work, we consider acetic, propionic, and butyric acid
SRT	Solids' retention time	d	Time the solid fraction of the flow spends in a tank e.g. the amount of time the microbial biomass spends in the colon
UGI	Upper gastrointestinal tract		Subsection of the gastrointestinal tract encompassing the passageway from the mouth to the start of the colon, i.e. the esophagus, the stomach, and the small intestine
USDA	United States Department of Agriculture		Acronym for government department that created the food central database
WD	Western diet		One of two diets within the clinical trial with the same ratios of carbohydrates, proteins, and fats and and the necessary calories to remain in energy balance, this diet was designed to be deficient in microbiome-fermentable substrates
wt_{cell}	Wet weight per cell	$g_{wet\ wt}$ $cell^{-1}$	Average wet weight per cell – calculated using cell dimensions and density
X	Biomass	gCOD	Biomass within the colon
X_M Factor	Methanogen solids-concentration factor	$cells_{colon}$ $cells_{feces}$	A factor calculated using the DAMM model that estimates the amount of methanogens in the

			colon relative to the amount measured in the feces
X_M^0	Initial methanogen biomass in colon	gCOD	A starting amount of methanogen microbial biomass within the colon estimated using qPCR measurements in fecal samples
α_N	Absorption fraction of nutrient *N*	$g_{abs}\ g_{ingested}^{-1}$	Fraction of absorbed mass within the UGI of the total ingested amount for specific nutrient
σ_{est}	Standard error of the estimate	gCOD d^{-1}	Estimation of the accuracy of metabolizable COD predictions
τ	Kendall's coefficient of concordance		Indicator of proportional bias between methods

Introduction

The microorganisms that live within the human colon metabolize undigested food and contribute to the energy available to the human host from ingested food (1). Gut microbes use hydrolases that human cells do not possess to break down complex food polymers, and then bacteria ferment the monomers to simpler products that can be easily absorbed in the colon by the human host or can be excreted in feces (1,2). The literature highlights numerous connections between colonic microorganisms and human health and disease, including metabolic diseases such as obesity and diabetes (3–6), autism (7), and even psychological/emotional states (8). In humans, the exact mechanisms by which microbes influence the development of or protection from obesity are not established, though qualitative relationships between specific microbes and obesity are beginning to be investigated (9).

A fundamental concept within the study of human energy balance is metabolizable energy (E_m), which is defined as the energy from food that is available for the human's metabolic processes (10). However, in environmental microbiology, the standard measurement for microbial substrates is chemical oxygen demand (COD) (11). COD is the measured mass of oxygen required to completely oxidize organic carbon and can be represented more generally as electron equivalents (11); the use of electron equivalents is important in environmental microbiology because it can be used with microorganisms which, unlike human cellular respiration, are not limited to oxygen as an electron acceptor. In our prior work, we developed a set of regression equations to convert between E_m and metabolizable chemical oxygen demand (COD_m) (12).

In the late 19th century, Atwater and co-workers developed an empirical relationship to calculate E_m as a fraction of gross energy (E_g), defined as the total combustible energy within food items (13–15). The Atwater system uses a single factor to convert the mass of food (grams)

directly to the E_m (kcal or kJ) for each macronutrient, i.e., proteins, carbohydrates, and fats; the factors are 4 kcal g^{-1} for proteins, 4 kcal g^{-1} for carbohydrates, and 9 kcal g^{-1} for fats (13,15). Due to their simplicity and reasonable accuracy, the Atwater factors remain the most commonly used method to calculate E_m (14) and there have been efforts to improve the factors by accounting for fiber fermentation (16).

The three Atwater factors were developed empirically by subtracting energy of combustible gas, fecal, and urinary excretions from measurements of the heat of combustion of total ingested proteins, carbohydrates, and fats (14). The method is unable to account for interpersonal variations, including differences in diet that affect the colonic microbiome. In particular, the Atwater method lumps many metabolic factors into one parameter. A key "lumped-in" factor is the organic acids produced by the colonic microbiome and then absorbed and metabolized by the human host. The Atwater factors *de facto* assume that the microbial contribution is consistent for all persons, even though the microbial community is known to vary with sex, age, race, geographical region, genetics, the health of the host, and, especially, diet (17–22). Several studies found that the Atwater E_m calculation systematically overestimates or underestimates E_m for various food items by not accounting for differences that affect the gut microbiome (10,13,23–26). In addition, the Atwater approach does not separate the absorption of dietary substrates in the upper gastrointestinal tract from the lower gastrointestinal tract; thus, it does not explicitly include the organic acids produced by the metabolism of the colonic microbiome.

A model that considers the microbial contribution to host metabolizable energy – by tracking food-related energy throughout the digestion and metabolic processes – can be used to understand and quantify the interactions between the gut microbiome and the human body. Here, we describe our Digestion, Absorption, and Microbial Metabolism (DAMM) mathematical model,

which tracks the progression of ingested macronutrients as they advance through the host's digestive tract until they are subsequently absorbed and metabolized by organs and tissues or excreted. Most importantly, the integrated mathematical model explicitly accounts for the contribution to COD_m – which can be directly converted to E_m (12) – by the colonic microbial community. Using the DAMM mathematical model, we quantify how diet affects the products of microbial metabolism and the total metabolizable COD_m (and, by conversion, kcal (12)) absorbed by the host. This mathematical model provides novel insights into the role of microbial metabolisms in host digestion while improving accuracy of metabolizable COD_m predictions found in alternate prediction methods (15).

Methods

Digestion, Absorption, and Microbial Metabolism (DAMM) model concept and structure

The DAMM model was developed using bioreactor principles, with the model's coefficient values, definitions, and sources detailed in the **Supplemental Material**. A flow chart illustrating the primary processes considered in the DAMM mathematical model is shown in **Figure 1**. The principal function of the model is to predict the metabolizable chemical oxygen demand (COD_m) that is absorbed in the Upper Gastrointestinal Tract (UGI) and Lower Gastrointestinal Tract (LGI).

While the DAMM mathematical model is founded on previously published versions of the digestion model (27), it has several improvements. Specifically, we included a more comprehensive description of the consumed macronutrients, refined the stoichiometry and kinetics of the colonic microbial community, incorporated methanogenesis as a potential reaction, and considered absorption of short-chain fatty acids (SCFAs) by colonic epithelial cells. These

changes are illustrated in **Figure 1**, along with the output streams to the labeled Absorption partition. Here, we discuss the model's diet inputs, other inputs, processes, and outputs.

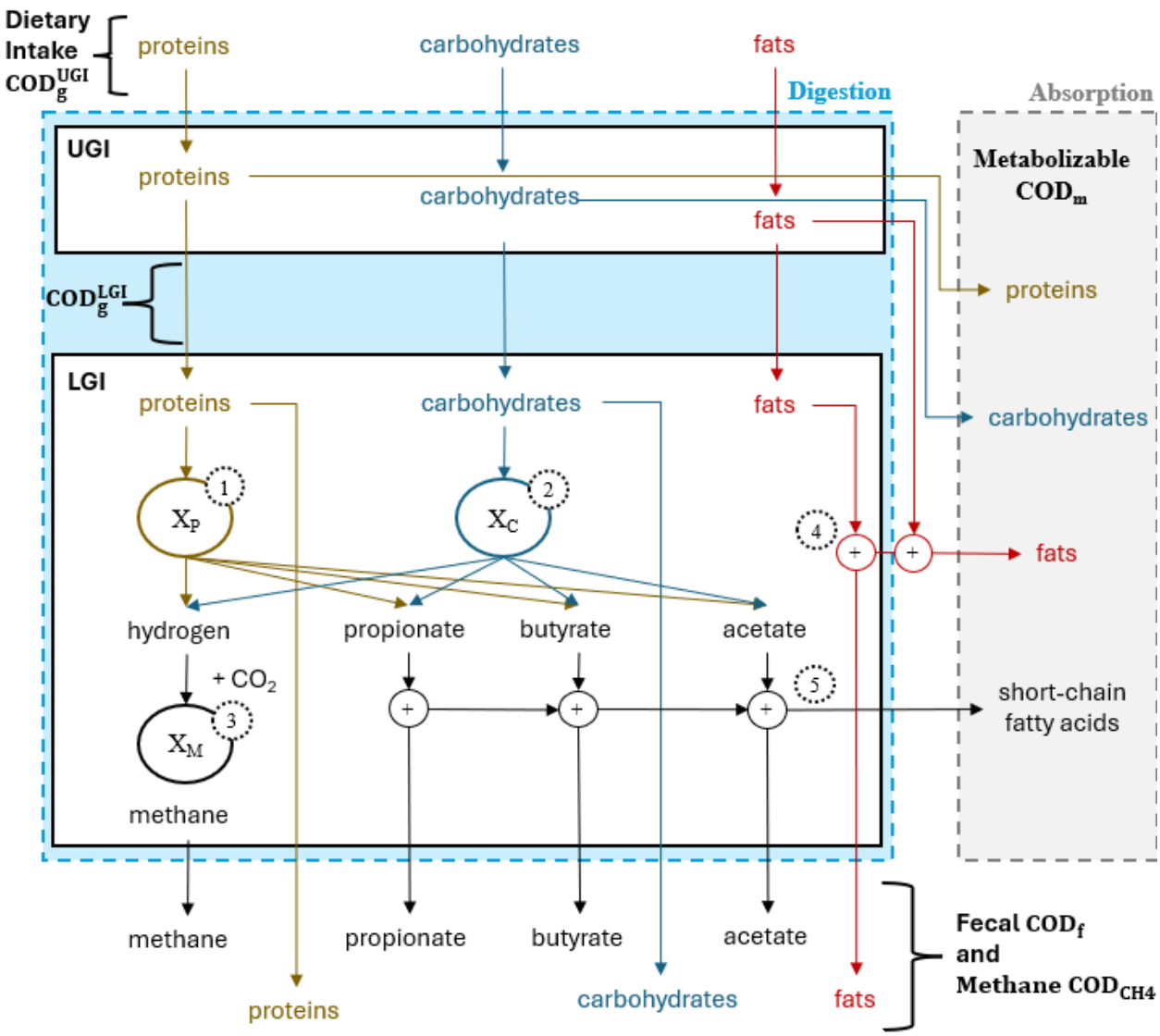

Figure 1: Flow chart of the Digestion, Absorption, and Microbial Metabolism (DAMM) mathematical model.
The diagram tracks proteins, carbohydrates, and fats as they travel through the digestive tract and then are output either as feces or gas excretions or absorbed by the human body. Processes labeled with numbers in dotted circles are 1) hydrolysis and fermentation of proteins, 2) hydrolysis and fermentation of carbohydrates, 3) methanogenesis, 4) absorption of fats, and 5) absorption of short-chain fatty acids (SCFAs). The blue dotted outline defines the control volume for the digestive tract, while grey is the rest of the human body. UGI and LGI are the upper and lower gastrointestinal compartments, respectively. COD is chemical oxygen demand, while subscripts refer to the following: g – gross, m – metabolizable, f – fecal, and CH_4 – methane.

Dietary intake as chemical oxygen demand converted from grams of ingested macronutrients

The DAMM model's diet input is the daily mass of macronutrients (proteins, carbohydrates, and fats) consumed by the participant in gCOD d^{-1} and labeled as COD_g^{UGI} (top of **Figure 1**). We used Equation 1 to convert the mass of each food item (amt_{food} [$g_{food\ wet\ weight}$ d^{-1}]) to the daily gross COD of each nutrient ($COD_g^{nutrient}$ [gCOD d^{-1}]) for the input.

$$COD_g^{nutrient}\left[\frac{gCOD_{nutrient}}{d}\right] = amt_{food}\left[\frac{g_{food\ wet\ weight}}{d}\right]\left(f_{nutrient}\left[\frac{g_{nutrient}}{g_{food\ wet\ weight}}\right]\right)\left(COD_{nutrient}\left[\frac{gCOD_{nutrient}}{g_{nutrient}}\right]\right) \quad (1)$$

The mass fraction of each macronutrient (amino acids, lipids, sugars, starch, and fiber) in the food item ($f_{nutrient}$ [$g_{nutrient}$ $g_{food\ wet\ weight}^{-1}$]) was estimated using the United States Department of Agriculture (USDA) Food Data Central Database (28); the database contains the gram amount of individual amino acids, lipids, sugars, starch, and fiber quantities per 100 grams for thousands of food items and was used by the menu creation software when designing the two clinical trial diets (29). The daily ingested mass of each macronutrient in a specific food item was determined by multiplying the daily intake of that food item by the fraction of the macronutrient it contains. This was then converted to $COD_g^{nutrient}$ by multiplying the value by the specific chemical oxygen demand of the nutrient ($COD_{nutrient}$ [gCOD g^{-1}]). The values for $COD_{nutrient}$ were calculated from the chemical formula of each macronutrient using established procedures described in our prior publications (11,12).

Using Equation 1 for all food items ingested per day resulted in a comprehensive breakdown of the composition of the diet since the ingested COD of each macronutrient was known. This level of detail for a diet is a substantial advancement from the prior versions of our

digestion model (22,27), which aggregated the diet input into these categories: protein, fat, non-fiber carbohydrate, and fiber carbohydrate.

Measured colonic transit time and initial methanogen biomass

We input into the DAMM model two other state variables: colonic transit time (CTT [d]) and an estimate of the initial methanogen biomass within the colon (X_M^0 [gCOD]). During our clinical trial (22), the details of which are listed in a later section, the CTT was measured using a radio-transmitting capsule (SmartPill™; Medtronic, Minneapolis, MN) that recorded internal temperature, pressure, and pH (22,29,30). The data were analyzed to determine CTT for each participant on each diet; CTT was identified as a parameter with a complex and highly variable relationship to diet for individuals. Within the model, CTT is incorporated into the equations for microbial production rates and SCFA absorption.

Methanogenesis does not occur in all individuals and depends on the presence of methanogens within the colonic microbial community (31,32). To model methane (CH_4) production, the DAMM model requires an initial estimate of the methanogen biomass COD (X_M^0 [gCOD]). We used data generated with quantitative polymerase chain reaction (qPCR) targeting the gene for the methyl coenzyme M reductase (*mcrA*) to measure the gene copy number of methanogens for each participant's fecal samples (31). From the *mcrA* gene copy number, we estimated an initial methanogen biomass using the following equation:

$$X_M^0[gCOD] = mcrA[copy\#]\left(\frac{1}{N_{copy}}\left[\frac{cell}{copy\#}\right]\right)\left(wt_{cell}\left[\frac{g_{wet\,wt}}{cell}\right]\right)\left(f_{dry}\left[\frac{g_{dry\,wt}}{g_{wet\,wt}}\right]\right)\left(f_{org}\left[\frac{g_{org\,dry\,wt}}{g_{dry\,wt}}\right]\right)\left(COD_{biomass}\left[\frac{gCOD}{g_{org\,dry\,wt}}\right]\right) \quad (2)$$

Methanobrevibacter smithii represented the methanogen population, based on its being prominent in the intestines (32,33) and detected in our study (31). We estimated the organic dry weight per

cell of *M. smithii* as $2x10^{-13}$ g $cell^{-1}$ using "rod" dimensions (length = 1.5 µm, diameter = 1 µm, density = 1 g cm^{-3} (34)) and assumed 20% of the cell is organic dry mass (11). The methanogen biomass was represented using the formula $C_5H_7O_2N$ (25), making the specific biomass $COD_{biomass}$ [gCOD g^{-1}] 1.42 gCOD g^{-1} for the methanogens. Parameters used in the calculations are summarized in **Table 1**, and calculated values by participant are in **Supplemental Material Table 1**.

Table 1: Methanogen-specific parameters
List of methanogen-specific parameters utilized in Equation 2 to calculate initial methanogen biomass (X_M^0) from the methyl coenzyme M reductase (*mcrA*) copy number measurements. Each parameter has its value with units, a description of the parameter's purpose, and the source for the value.

Variable	Value	Units	Description	Source
N_{copy}	1	copy# $cell^{-1}$	Gene copy # per cell for methanogens	(35)
wt_{cell}	1.2×10^{-12}	$g_{wet\ wt}$ $cell^{-1}$	Cell weight V*ρ, assume a cylinder for volume: h = 1.5 µm, d = 1 µm then V = $1.2x10^{-12}$ cm^3/cell and ρ = 1g/cm^3	(34)
f_{dry}	0.2	$g_{dry\ wt}$ $g_{wet\ wt}^{-1}$	Dry weight per gram wet weight	(11)
$COD_{biomass}$	1.42	$gCOD_{meth}$ $g_{org\ dry\ wt}^{-1}$	Specific biomass COD, calculated with cell chemical formula as $C_5H_7O_2N$	(11,27)
f_{org}	0.9	$g_{org\ dry\ wt}$ $g_{dry\ wt}^{-1}$	Organic fraction of dry weight	(11)

Absorption of proteins, carbohydrates, and fats in the upper gastrointestinal tract

The model's UGI compartment estimated the absorption of proteins, fats, and carbohydrates in the small intestine before entering the colon (UGI portion of **Figure 1**). The UGI model was adapted from a model used to simulate the human digestive tract post-colonic-resection surgery (27). Because the participants in the parent clinical trial had an intact GI tract, we removed

the effect of the loss of a portion of the small intestine, which gave the rate of COD absorption in the UGI (COD_m^{UGI} [gCOD d^{-1}]) as:

$$COD_m^{UGI}{}_N = \alpha_N COD_g^{UGI}{}_N \tag{3}$$

which can be applied for any macronutrient *N* (i.e., fiber, starch, or any of the sugars, amino acids, or saturated and unsaturated lipids). The variable α_N represents the absorption fraction of nutrient *N,* and the variable $COD_g^{UGI}{}_N$ is the total ingested amount of the nutrient, in gCOD d^{-1}. Specific UGI-digestibility fractions for each nutrient were taken from the literature (27,36–38); **Supplemental Material Table 2** presents the UGI constants.

Equations 4 and 5 give the steady-state nutrient-COD balance for the UGI:

$$\frac{d}{dt} COD^{UGI}{}_N = 0 = COD_g^{UGI}{}_N - COD_g^{LGI}{}_N - COD_m^{UGI}{}_N \tag{4}$$

$$COD_g^{LGI}{}_N = COD_g^{UGI}{}_N (1 - \alpha_N) \tag{5}$$

$COD_g^{UGI}{}_N$ is the total ingested nutrient COD, $COD_g^{LGI}{}_N$ is the nutrient COD going into the colon, and $COD_m^{UGI}{}_N$ is the nutrient COD absorbed within the small intestine. The model operates on the timescale of a 24-hour day, while the orocecal transit time (time from mouth to the beginning of the colon) is approximately 5 hours (39,40); thus, we assumed no storage of nutrients within the UGI ($\frac{d}{dt} COD^{UGI}{}_N = 0$), which means that the nutrient was either absorbed in the UGI or entered the colon. The output from the UGI compartment was the input for the LGI compartment.

Lower gastrointestinal tract mass balance

The LGI compartment encompasses the physiological processes of the colon and the colon's microbiome: microbial fermentation reactions of proteins (**Figure 1**: process 1) and carbohydrates (process 2) to SCFA products, methanogenesis (process 3), absorption of fat within the colon (process 4), and absorption of SCFAs within the colon (process 5). We represented the

colon as a single continuously stirred reactor (CSTR) with a solids' retention time (SRT) equivalent to the measured CTT (25). We also tested a plug-flow reactor but found no statistical difference between the CSTR and plug-flow reactor results, consistent with the findings of Moorthy and colleagues (41,42). Thus, we used the CSTR configuration.

A CSTR mass balance equation was used to solve for the effluent mass leaving the LGI compartment:

$$\frac{d}{dt}COD^{LGI}{}_{N} = R_{ut-N} + COD_{g}^{LGI}{}_{N} - COD_{f\,N} \tag{6}$$

The variable $R_{ut\text{-}N}$ [gCOD d^{-1}] is the total utilization rate per day for the macronutrient *N*; we included the five processes described in **Figure 1** in this term. The last two terms express the influent ($COD_g^{LGI}{}_N$ [gCOD d^{-1}]) and effluent flow ($COD_{f\,N}$ [gCOD d^{-1}]), respectively. Due to the perfectly mixed assumption of the CSTR configuration, the LGI effluent concentration is equivalent to the concentration within the reactor; thus, the LGI effluent flow is equivalent to the concentration within the reactor divided by the solids' retention time.

Microbial hydrolysis and fermentation of proteins and carbohydrates

The LGI model considers microbial hydrolysis and fermentation of proteins and carbohydrates. The microbial utilization of protein is labeled process 1 in **Figure 1**. We considered protein metabolism in the LGI to occur in two stages: hydrolysis, which is the rate-limiting step, followed by fermentation that produces H_2, propionate, butyrate, and acetate. A mixed second-order rate described the rate of protein hydrolysis ($R_{P\,hyd}$ [$gCOD_N$ d^{-1}]):

$$R_{P\,hyd} = k_{P\,hyd}(N)\left(X_{P,N}\right) \qquad \text{where } N \text{ is any amino acid.} \tag{7}$$

The variables $k_{p\,hyd}$ [$gCOD_X^{-1}$ d^{-1}], *N* [$gCOD_N$], and $X_{P,N}$ [$gCOD_X$] are, respectively, the second-order rate constant for protein hydrolysis, the amount of COD for amino acid *N* in the colon, and

the current amount of protein-degrading biomass COD using substrate *N* in the colon. Hydrolysis constants are listed in **Table 2**.

Table 2: Kinetic parameters
List of kinetic parameters for methanogenesis, carbohydrate, and protein hydrolysis and fermentation utilized in Equations 3-12 to calculate the amounts of microbially produced products within the LGI compartment of the DAMM model.

Variable	Value	Units	Description	Source
$k_{F\ abs}$	0.48	d^{-1}	First-order absorption coefficient for fat in the LGI	(27)
$k_{C\ ferm}$	10	$gCOD^{-1}\ d^{-1}$	Second-order kinetic coefficient for fermentation of simple sugars like glucose or fructose	(11)
$k_{C\ hyd}$	1	$gCOD^{-1}\ d^{-1}$	Second-order kinetic coefficient for hydrolysis of complex carbohydrates like fiber or resistant starch	(11)
$k_{P\ hyd}$	5	$gCOD^{-1}\ d^{-1}$	Second-order kinetic coefficient for hydrolysis of proteins into amino acids	(11)
k_M	0.5	$gCOD^{-1}\ d^{-1}$	Second-order kinetic coefficient for methanogenesis	(11)
$K_{scfa\ abs}$	0.02	d	Half-saturation constant for absorption of SCFAs in the LGI	(30)

For utilizations of fiber and resistant starch (complex carbohydrate), we assumed the same two-step process, but the products were limited to the three main SCFAs: propionate, butyrate, and acetate. However, simple carbohydrates do not require hydrolysis; thus, we defined a separate rate equation for simple carbohydrate fermentation. Carbohydrate hydrolysis and fermentation are collectively labeled as process 2 in **Figure 1**. We used the mixed second-order rate equation to describe the hydrolysis of complex carbohydrates and the fermentation of simple carbohydrates.

$$R_{C\ hyd} = k_{C\ hyd}(N)\left(X_{C,N}\right) \tag{8}$$

where N is a fiber or starch

$$R_{C\ ferm} = k_{C\ ferm}(N)\left(X_{C,N}\right) \tag{9}$$

where N is a sugar.

The variables $k_{C\,hyd}$ [$gCOD_X^{-1}$ d^{-1}], $k_{C\,ferm}$ [$gCOD_X^{-1}$ d^{-1}], and $X_{C,\,N}$ [$gCOD_N$] are, respectively, the second-order complex carbohydrate hydrolysis rate constant, the second-order simple carbohydrate fermentation rate constant, and the current amount of carbohydrate-degrading biomass COD within the colon using carbohydrate N as a substrate. In Equation 8, N [$gCOD_N$] is either fiber or starch COD in the colon, and in Equation 9, N [$gCOD_N$] is simple-carbohydrate COD in the colon. Hydrolysis and fermentation constants are listed in **Table 2**.

We used an energy-and-electron-balancing method (29) to develop the stoichiometry matrix for carbohydrate and protein fermentation. The product ratios for each amino acid nutrient were taken from Ramsay et al. (43). Product ratios for carbohydrate fermentation were the same as in Marcus et al. (27). To include biomass synthesis in the stoichiometry, we assumed the fraction of donor electrons utilized for cell synthesis was equal to 0.2 (i.e., $f_s = 0.2$ e^- to synthesis/e^- from the donor), a value estimated from known values of anaerobic fermenters (11). In the reaction stoichiometry, any type of microbial biomass was represented using the empirical chemical formula $C_5H_7O_2N$. The stoichiometry matrix in gCOD is in **Supplemental Material Table 3**.

Methane production if methanogens are present in the lower gastrointestinal tract

Though methanogens are low-abundance species within the gut microbiome, they are one of three identified microbial groups that consume H_2, which strongly influence microbial interactions (1,20,44). All known methanogen species in the human gut oxidize H_2 and reduce CO_2 to produce CH_4, which is then excreted by the human host (**Figure 1**: process 3). Within the clinical trial, we measured the total CH_4 released by the human over the course of 23 hours in a whole-room indirect calorimeter (45). For CH_4 calculation, the equation for methanogenesis stoichiometry was developed using the same method detailed in the carbohydrate and protein

hydrolysis and fermentation sections; the complete stoichiometry table is in **Supplemental Material Table 3**. Similarly, we used the same mixed second-order rate as for the other microbial processes.

$$R_M = k_M(H_2)(X_M) \tag{10}$$

The variables k_M [gCOD^{-1} d^{-1}], H_2 [gCOD], and X_M [gCOD] represent, respectively, the methanogenesis second-order rate constant (**Table 2**), the COD equivalent of H_2 produced by microbes present in the colon, and the COD of methanogen biomass.

Absorption of short-chain fatty acids and fats in the lower gastrointestinal tract

For carbohydrates and proteins, a human's direct absorption (COD_m^{UGI}), i.e., not requiring hydrolysis and fermentation by the gut microorganisms, occurs in the UGI tract (**Figure 1**). Direct absorption of fats (**Figure 1**) is not restricted to the UGI. We define the rate of fat absorption, $R_{F\ abs}$ [gCOD$_N$ d^{-1}], in the LGI using first-order kinetics:

$$R_{F\ abs} = k_{F\ abs}N \tag{11}$$

In Equation 11, N [gCOD$_N$] is the mass of a specific fat, and $k_{F\ abs}$ [d^{-1}] is the first-order rate constant. We calculated the absorption of microbially produced SCFAs within the LGI (**Figure 1**: process 5). In the prior version of the digestion model (27), we assumed the absorption of SCFAs within the colon is a constant proportion of 95%, but we also showed that the amount of SCFAs absorbed from the colon was affected by the CTT (19). We computed the fraction of SCFA absorption using a saturation relationship based on CTT:

$$e_{scfa\ abs} = \frac{CTT}{CTT + K_{scfa\ abs}} \tag{12}$$

which is illustrated in **Supplemental Material Figure 1**. In Equation 12, $e_{scfa\ abs}$ is the mass of absorbed SCFAs normalized to the total mass of produced SCFAs, CTT [d] is the colonic transit time, and $K_{scfa\ abs}$ (**Table 2**) is the CTT when 50% of SCFAs are absorbed.

DAMM model validation – clinical trial data and statistics

We evaluated the DAMM model's capabilities by comparing its outputs to data from a clinical trial (NCT02939703) designed to quantify the impact of the gut microbiome on human energy balance (22,29). Within the clinical study, 17 healthy men and women consumed two diets in a randomized crossover design. Each diet was consumed at home for 11 days and then for 11 days while the participant was domiciled in a metabolic ward. A ≥ 14-day washout period occurred between the two diet periods. The microbiome enhancer diet (MBD) was a "whole-foods" diet high in dietary fiber and resistant starch but minimally processed foods. The MBD was designed explicitly to maximize the delivery of fermentable dietary substrates to the colon. In contrast, the western diet (WD) was high in processed foods and low in dietary fiber and resistant starch. Both diets were designed to provide energy (kcals) to match the participant's measured energy expenditure over 6 days in a whole-room calorimeter to achieve energy balance on both diets. Meals were designed by a Registered Dietitian using research-grade software (ProNutra Version 3.5, Viocare, Inc, Princeton, NJ) and prepared in a metabolic kitchen to precisely deliver the nutrients as designed. Adherence was >99% on both diets, and any food not eaten was weighed so that the actual nutritional intake could be calculated. Fecal samples were collected for the 6 days when the participants resided within the whole-room calorimeter.

We used several statistical metrics to evaluate the DAMM model's performance. For direct comparison between measured and predicted values, we evaluated the accuracy of the predictions using the coefficient of determination (R^2) and the standard error of the estimate (σ_{est}) relative to the identity line (X = Y). When comparing the metabolizable COD_m predictions provided by the DAMM model with the Atwater constants, we used a Bland-Altman plot to visualize the agreement between the predictions and measurements. We looked at the systemic bias by doing a one-sample

t-test against the zero difference between methods and calculating Kendall's coefficient of concordance (τ) for proportional bias. All statistics were computed using the SciPytools package in Python (46).

Results & Discussion

Model predicts microbial contribution to metabolizable COD from upper and lower gastrointestinal tracts

The DAMM model tracks the flow of COD from macronutrients as they move through the upper and lower gastrointestinal tracts. **Figure 2A** presents the average daily distribution of COD – with pie plots showing the breakdown into protein, carbohydrate, fat, and SCFAs – across the inlet and outlet streams depicted in **Figure 1** for both diets. The dietary intake, i.e., gross COD for the UGI inlet (COD_g^{UGI}), had an average value of 630 ± 105 gCOD d^{-1}. The DAMM predicted that 102 ± 21 gCOD d^{-1} (16.2 ± 2.1% of dietary intake) continued into the colon, while only 26 ± 8 gCOD d^{-1} (4.2 ± 0.9% of dietary intake) was excreted as feces or gas.

Figure 2B combines the metabolizable COD (COD_m) from the UGI and the LGI, and it segments the bars by proteins, carbohydrates, fats, and SCFAs. The model predicts an average COD_m of 93.0 ± 4.1%, within which approximately 85% came from the UGI and 15% from the LGI. SCFAs absorbed from the LGI contribute an average of 43.6 ± 12.0 gCOD d^{-1} to the metabolizable COD; this is 7.4% of the total COD_m and roughly equivalent to 140 kcal d^{-1}. While protein, carbohydrate, and fat absorption in the UGI largely occurs with specific transporters after being broken down by enzymes (47), absorption in the LGI occurs after fermentation to products such as microbially produced SCFAs (48). By separating UGI and LGI absorptions, the DAMM model accounts for the distinct pathways for metabolizable COD; the prediction of microbial

fermentation products in the LGI means that in the future, this information can be separately input into existing models that predict changes in body energy stores (49) and allow us to consider the microbial contribution explicitly.

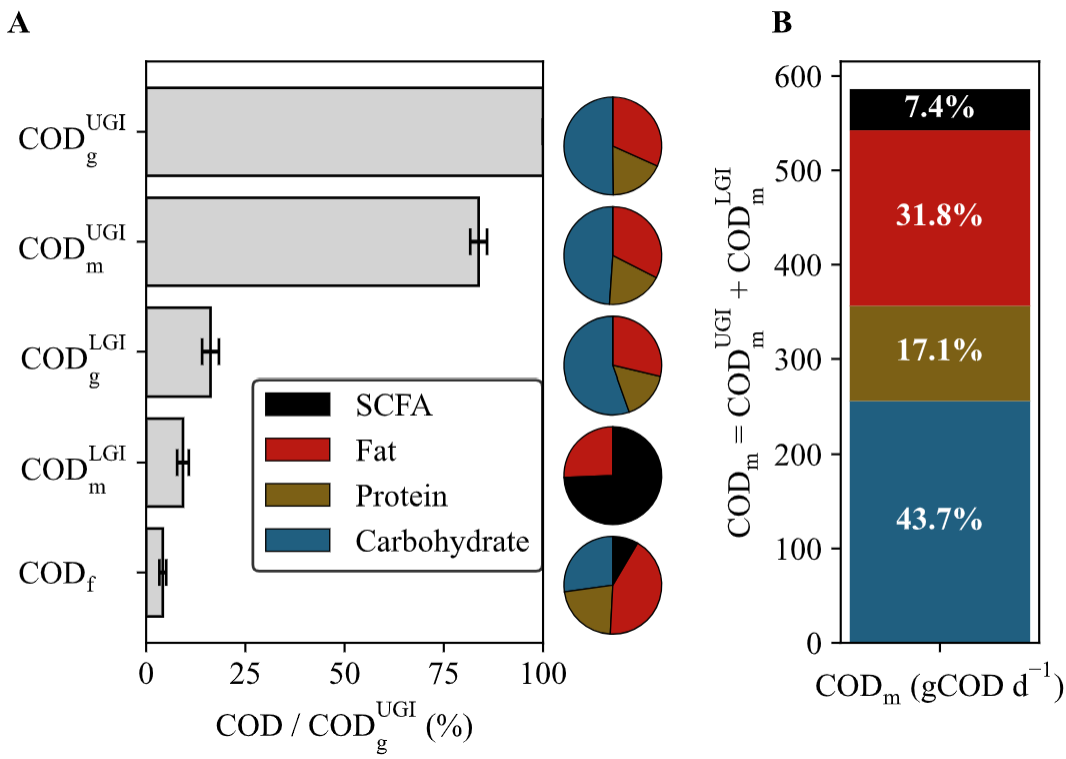

Figure 2: Mass balances for chemical oxygen demand (COD) in upper and lower gastrointestinal (UGI and LGI) tracts.
A) The percent of the dietary intake (%) that each input and output stream of the UGI and LGI compartments within the Digestion partition of the DAMM model. Bars represent the average ± standard deviation for both diets. The top three bars - COD_g^{UGI}, COD_m^{UGI}, and COD_g^{LGI} - are the inputs/outputs for the UGI, while the bottom three bars - COD_g^{LGI}, COD_m^{LGI}, and COD_f - are the inputs/outputs for the LGI. The fractions of SCFA, Fat, Protein, and Carbohydrate for each bar are shown on the pie charts directly to the right. **B)** A stacked bar chart of the average amounts of SCFA, Fat, Protein, and Carbohydrates within the DAMM predicted total metabolizable COD. Percentages of the total are listed on each bar segment. Subscripts for COD refer to the following: g – gross, m – metabolizable, and f – fecal.

DAMM model captures interindividual variation of fecal SCFAs and biomass on diets

Inputs from a prior clinical trial (22) were used to generate DAMM model outputs. In that trial, two diets were administered in random order to each participant (crossover study design).

Both diets had similar percentages of proteins, carbohydrates, and fats, but the MBD was designed to encourage fermentation in the LGI by having a higher amount of carbohydrates that are not digestible by the human host than the WD. **Figure 3** depicts the DAMM model's predicted metabolizable COD from total absorbed SCFAs, acetate, butyrate, and propionate. The predictions for each diet were significantly different, mirroring the directionality that was observed in the clinical trial (higher SCFAs in serum and feces on the MBD as compared to the WD). The butyrate values were the most similar, having a difference of only 3.3 gCOD d^{-1}, which is roughly 10 kcals d^{-1}. The average total predicted metabolizable COD from SCFAs was 51.9 ± 9.8 gCOD d^{-1} on the MBD and 33.8 ± 4.4 gCOD d^{-1} on the WD, which are 5% and 10% of the total metabolizable COD, respectively.

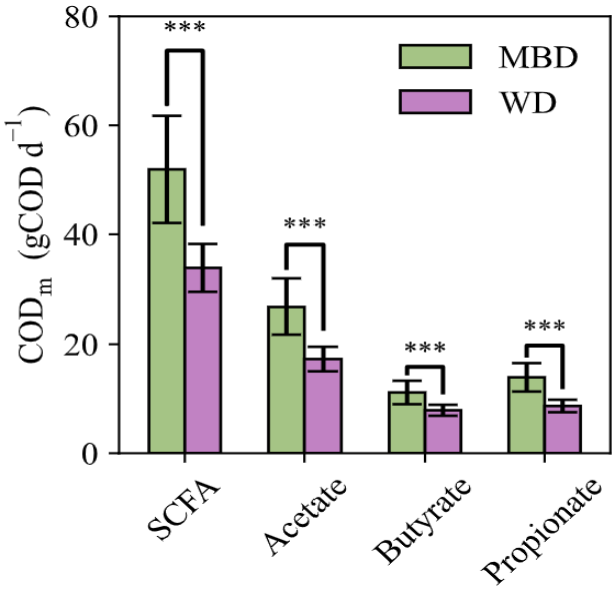

Figure 3 : Predictions for short-chain fatty acid (SCFA) metabolizable chemical oxygen demand (COD_m) by diet.
Bars represent the mean ± standard deviation of all participants for each diet. Statistical significance was determined using a t-test: "***" indicates $p < 0.001$. Brackets above the bars highlight the comparisons between the two diets. Comparisons were performed for acetate, butyrate, propionate, and SCFA which is the sum of the three.

We cannot compare these predictions to measurements, because the clinical study could not directly measure SCFAs absorbed in the colon; however, the study measured the following SCFAs in the feces: acetate, propionate, and butyrate. The SCFA samples were from the 6-day composite fecal sample and the measurements were converted to the daily fecal COD (22). **Figures 4A** and **4B** compare the DAMM model's daily fecal COD predictions for acetate, butyrate, and propionate for all participants versus the measurements. Apart from butyrate on the MBD, the predictions for SCFA fecal COD have similar scale and variation as the measurements. T-tests were run for each measurement and prediction pair, and all had p-values greater than 0.3, except for MBD butyrate where the p = 0.07 (**Figure 4A**).

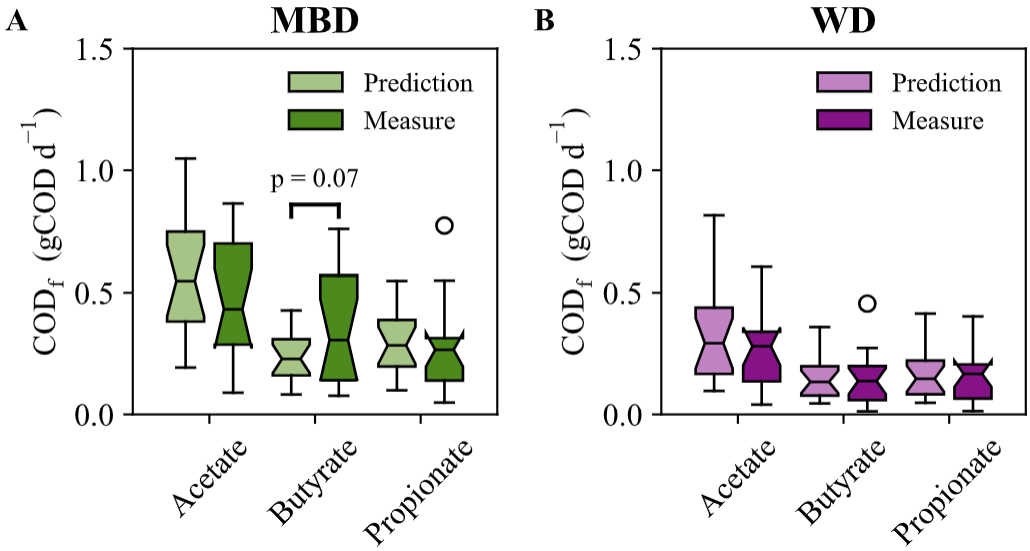

Figure 4 : Daily fecal short-chain fatty acid (SCFA) chemical oxygen demand (COD) boxplots comparing predictions and measurements by diet. **A)** Predictions for acetate, butyrate, and propionate fecal COD directly compared to the measurements for the microbial enhancer diet (MBD). **B)** Predictions for acetate, butyrate, and propionate fecal COD directly compared to the measurements for the western diet (WD). Statistical significance was determined using a t-test. All p-values were greater than 0.3, except when labeled on the plot.

Standard error of estimates (σ_{est}), relative to the 1:1 identity line, are listed in **Table 3** for acetate, butyrate, and propionate for the MBD and WD. The largest σ_{est}, 0.27 gCOD d^{-1} for butyrate on the MBD, is equivalent to 0.9 kcal d^{-1}; thus, the DAMM model predicted fecal SCFAs

within one kilocalorie per day. The good agreement between the fecal SCFA predictions and measured values, in magnitude and trend, supports the validity of the SCFA predictions from the DAMM model. Explicitly including SCFA production and absorption rates was key to the model's success. This is underscored by the fact that including CTT allowed the DAMM model to capture inter-individual variations in fecal-SCFA excretion rates; using a constant SCFA absorption ratio (e.g., 95%, as in the prior model (27)), would have yielded fecal SCFAs that spanned a range of less than 0.2 gCOD d^{-1} which we show in **Supplemental Material Figure 2**. While several factors can affect SCFA absorption (48,50,51), the accuracy of the DAMM predictions when using the CTT dependent absorption function show that CTT is an important factor.

Table 3: Standard error of estimate (σ_{est}) for DAMM predictions of fecal SCFA COD.
The error of estimate for SCFA predictions for the identity line i.e. that prediction should equal measurements.

SCFA Name	MBD σ_{est}	WD σ_{est}	Unit
Acetate	0.25	0.18	gCOD d^{-1}
Butyrate	0.27	0.12	gCOD d^{-1}
Propionate	0.17	0.10	gCOD d^{-1}

In addition to the SCFAs, the model also tracked the microbial growth that resulted from the defined reaction categories: carbohydrate fermentation, protein fermentation, and methanogenesis. Previous analyses on 16S rRNA gene qPCR measurements demonstrated a statistically significant increase in fecal biomass on the MBD as compared to the WD (31). As shown in **Figure 5A**, the model accurately captured this observation. DAMM predicted an

increase of 50 mgCOD for every gram of substrate COD that enters the colon on the MBD, compared with the WD.

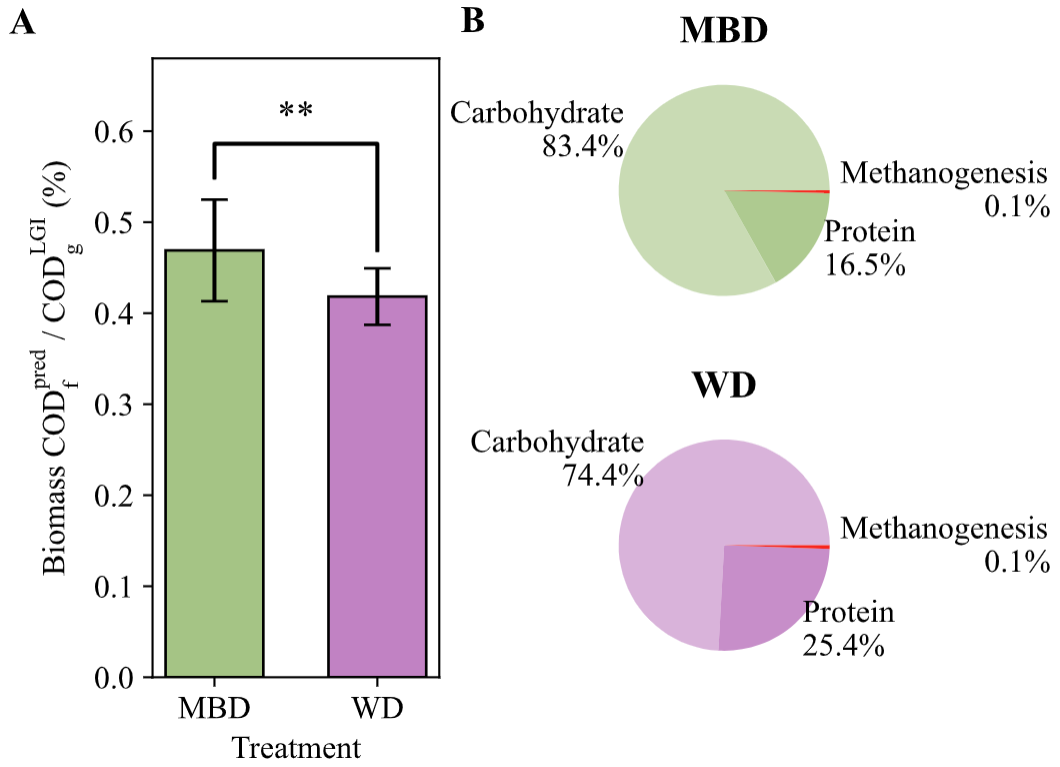

Figure 5: Fecal biomass chemical oxygen demand (COD) comparison between dietary treatments.
A) Direct comparison of the predicted fecal biomass COD (Biomass COD_f^{pred}) relative to the substrates COD coming into the colon (COD_g^{LGI}) on each diet. Bars represent the mean ± standard deviation of all participants for each diet. Statistical significance was determined using a t-test where $p = 0.002$. The "**" on the chart indicates $p < 0.01$. **B)** Pie charts display the fraction of predicted fecal biomass that is attributed to each of the three reaction categories: carbohydrate fermentation, protein fermentation, and methanogenesis for each diet. MBD is the microbiome enhancer diet, and WD is the western diet.

Figure 5B illustrates the average proportion of biomass attributed to each of the three reaction categories. For both diets, most of the biomass was from carbohydrate and protein fermentation, while biomass from methanogenesis was very small; methanogens are discussed more in the next section. Due to the higher amount of fiber and resistant starch on the MBD, which were not absorbed in the upper gastrointestinal tract, the percentage of fecal biomass from

carbohydrate fermentation was 10% higher for the MBD treatment compared to the WD. The greater availability of fiber-derived carbohydrates in the lower gastrointestinal tract resulted in increased carbohydrate fermentation by the microbial community.

Methane predictions support hypothesis that methanogens are present in biofilms in colon

The prior clinical trial measured fecal-methanogen abundance using qPCR targeting the *mcrA* gene (30), and we used these data to provide an initial estimate of methanogen biomass (X_M^0) for each participant (**Supplemental Material Table 1**). This X_M^0 was an input into the DAMM model to predict daily methane COD production (COD_{CH4}).

In **Figure 6A**, we compare the methane predictions with the measurements from the clinical trial for participants who produced significant methane (i.e., methane measurements exceeded 100 mL d^{-1}) (31,45). The predictions differ by at least an order of magnitude from the measurements for methane-producing participants. We calculated the standard error of the estimate (σ_{est}) relative to the identity line as 0.05 gCOD d^{-1}, with a coefficient of determination (R^2) greater than -4,000%. The very large systematic deviation in the model's predictions indicates that our initial X_M^0 estimates were too small. This conclusion is reinforced by **Figure 5B**, in which the fraction of methanogenesis was negligible compared to those for protein and carbohydrate fermentation.

The likely explanation for the systematic low values in **Figure 6A** is that most of the methanogens present in the colon were not in the feces but were accumulated in a biofilm on the intestine's epithelium. We evaluated this hypothesis by assuming that the true mass of methanogens was proportional to the methanogens measured in the feces, but larger by a solids-concentration factor (X_M Factor) that reflected that the methanogens had a larger SRT than the feces' CTT.

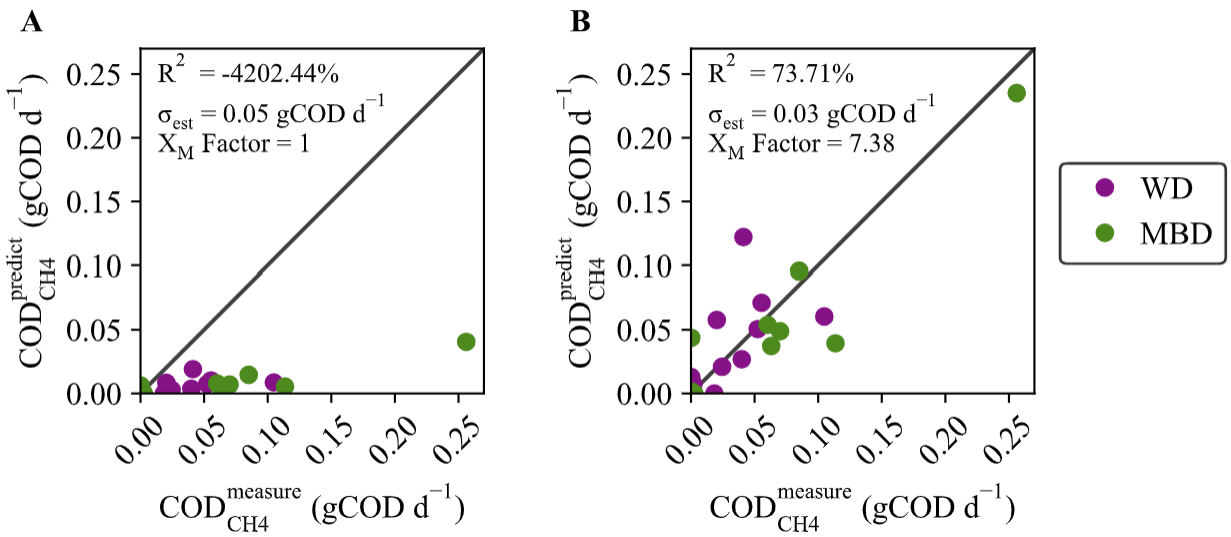

Figure 6: Predicted daily methane production in chemical oxygen demand (COD) compared to measurements for participants who generated measured methane. **A)** Comparing daily methane production ($COD_{CH4}^{predict}$) predictions to the ($COD_{CH4}^{measure}$) measurement when the initial methanogen biomass (X_M^0) is calculated directly from the *mcrA* qPCR copy numbers (X_M Factor = 1). R^2 for the identity line is -4202.44% and σ_{est} = 0.05 gCOD d^{-1}. **B)** Comparing $COD_{CH4}^{predict}$ to the $COD_{CH4}^{measure}$ when X_M^0 is proportional to the *mcrA* qPCR copy numbers times the factor 7.38 (X_M Factor = 7.38). R^2 for the identity line is 73.71% and σ_{est} = 0.03 gCOD d^{-1}. Data excludes one outlier where methanogens were measured in the feces, but the participant had minimal methane production. Symbol colors are by diet, where WD is the western diet and MBD is the microbiome enhancer diet.

We adapted Equation 2 to include X_M Factor to account for the accumulation of methanogens as a biofilm in the epithelium.

$$X_M^0[gCOD] = mcrA[copy\ \#]\left(\frac{1}{N_{copy}}\left[\frac{cell}{copy\#}\right]\right)\left(wt_{cell}\left[\frac{g_{wet\ wt}}{cell_{colon}}\right]\right)\left(X_M\ Factor\ \left[\frac{cells_{colon}}{cells_{feces}}\right]\right)\left(f_{dry}\left[\frac{g_{dry\ wt}}{g_{wet\ wt}}\right]\right)\left(f_{org}\left[\frac{g_{org\ dry\ wt}}{g_{dry\ wt}}\right]\right)\left(COD_{biomass}\left[\frac{gCOD}{g_{org\ dry\ wt}}\right]\right) \quad (13)$$

We used a grid-search algorithm that minimized the σ_{est} and calculated the optimum X_M Factor: 7.38 $cell_{colon}$ $cell_{feces}^{-1}$. **Figure 6B** shows that using a constant X_M Factor put all predicted values in the correct order of magnitude and eliminated systematic bias.

Allowing the methanogens to have a longer SRT within the colon dramatically improved results, which points to methanogens being retained in a biofilm in the mucus layer of the colon. Biofilms provide a stable environment in which methanogens, being slow growers, can thrive despite the relatively short CTT (1 – 2 days) (11). *Methanobrevibacter smithii*, the most common methanogen archaea in the human feces (31), has been shown capable of forming biofilms on different substrates (52,53), and it can also be retained in a biofilm formed by other microorganisms or by epithelium mucus (54). Having the methanogens in an epithelium biofilm would accentuate their interactions with the human host, including processing and absorption of SCFAs. Some evidence indicates that microorganisms in epithelial biofilms influence bowel inflammation and dysbiosis (55,56), while methanogens, specifically, *M. smithii*, have been linked to obesity (57) and anorexia (58). Further research is necessary, but the DAMM model creates a starting point to expand our understanding of how methanogens might contribute to health or disease.

DAMM model improves predictions for metabolizable chemical oxygen demand

The DAMM model estimates the metabolizable COD_m (which can be directly converted to metabolizable energy (12)) from the upper and lower gastrointestinal tracts. We compared the performance of the DAMM to the standard Atwater model (15) for predicting the metabolizable COD of all participants in the clinical study (22). **Figure 7** illustrates the predictive performance of the DAMM model (**Figures 7A** and **7C**) and the Atwater constants (**Figures 7B** and **7D**) compared to the actual COD_m (calculated as the difference between dietary intake and measured fecal COD). In **Figure 7A**, the DAMM model more accurately predicted the COD_m, as shown by the good fit to the identity line and the statistical metrics: $R^2 = 95.6\%$ and $\sigma_{est} = 20.6$ gCOD d^{-1}. The DAMM results are an improvement over the Atwater predictions (**Figure 7C**), which

consistently underestimated COD_m and had larger errors: R^2 = 88.5% and σ_{est} = 32.6 gCOD d^{-1}.

Table 4 quantifies similar differences when each diet is considered separately.

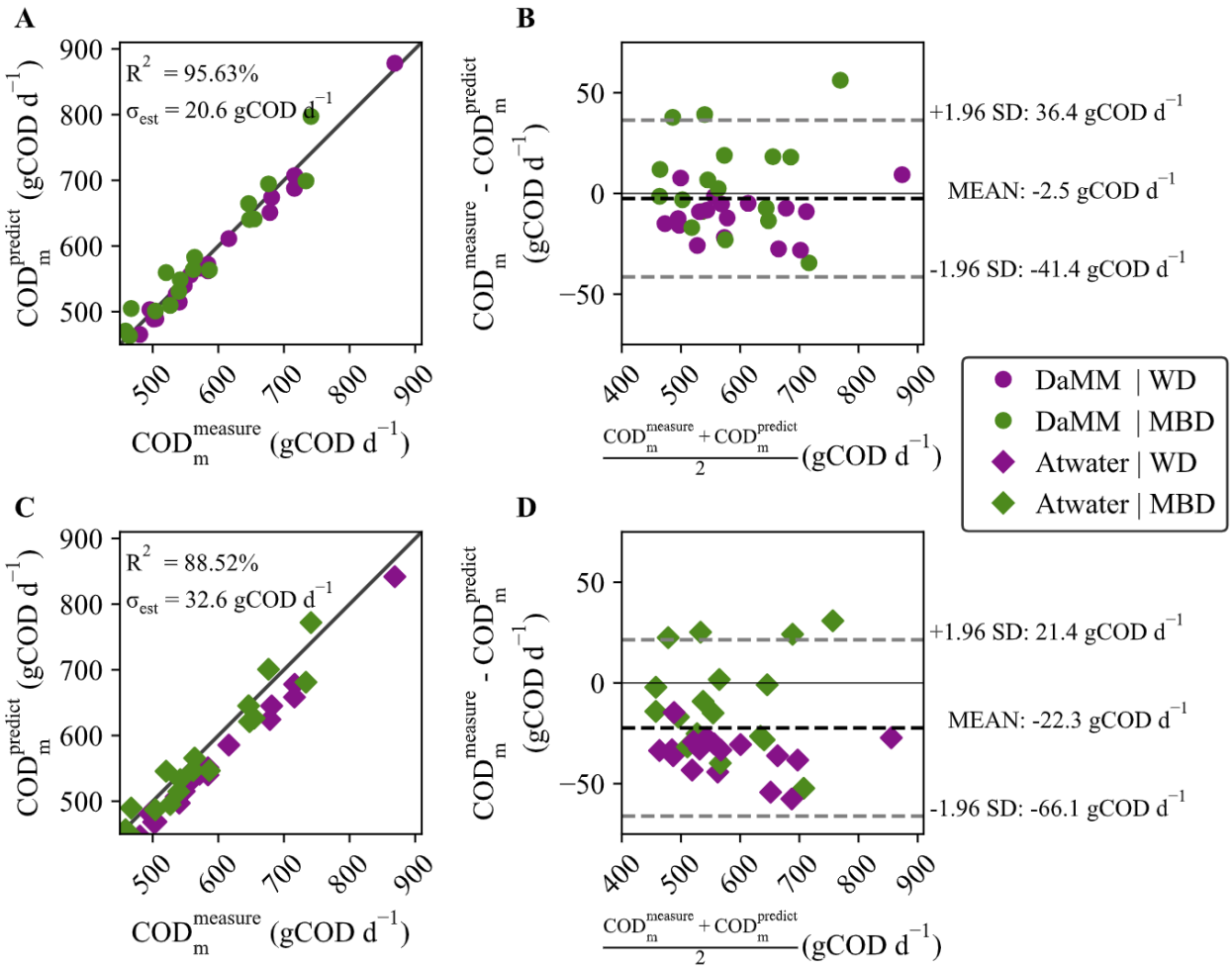

Figure 7 : Accuracy and bias evaluation of DAMM and Atwater metabolizable chemical oxygen demand (CODm) predictions.
A) Scatterplot of DAMM prediction versus measurement. The coefficient of determination (R^2) and standard error of estimate (σ_{est}) for the identity line are 95.63% and 20.6 gCOD d^{-1}. **B)** Bland-Altman plot showing the 95% confidence intervals at 36.4 gCOD d^{-1} to -41.4 gCOD d^{-1} with a mean of 2.5 gCODd^{-1} for the measurements and DAMM predictions. **C)** Scatterplot of Atwater prediction versus measurement. R^2 and σ_{est} for the identity line are 88.52% and 32.6 gCOD d^{-1}. **D)** Bland-Altman plot showing the 95% confidence intervals at 21.4 gCOD d^{-1} to -66.1 gCOD d^{-1} with a mean of -22.3 gCOD d^{-1} for the measurements and Atwater-constant predictions.

The Bland-Altman plots for the DAMM (**Figure 7B**) and Atwater constants (**Figure 7D**) further highlight the improvement in accuracy with the DAMM: The mean differences between predictions and measurements were only -2.5 gCOD d^{-1} for the DAMM, compared to -22.3 gCOD

d^{-1} for the Atwater constants, although the limits of agreement are roughly the same at approximately ± 40 gCOD d^{-1}. The Bland-Altman plots also show that, while the MBD treatment was evenly distributed, the WD clustered below the mean difference for both models.

We conducted a one-sample t-test to assess systematic bias and calculated Kendall's coefficient of concordance (τ) to examine proportional bias for each diet individually, as well as for the combined dataset that includes both treatments. Only the Atwater WD predictions had statistically significant bias: t-test = 3.37 gCOD d^{-1} and p = 0.002 (**Table 4**). According to the τ calculations for the mean difference and average of the measurements and predictions (**Table 4**), neither of the models had a proportional bias.

Table 4: Metabolizable chemical oxygen demand (COD_m) statistical metrics Includes coefficient of determination (R^2), standard error of estimate (σ_{est}), one sample t-test against the difference of the methods (t-test), and Kendall's coefficient of concordance (τ) to compare predictions to measurements for DAMM and Atwater models.

Model	Treatment	R^2 (%)	σ_{est} (gCOD d^{-1})	t-test (gCOD d^{-1})	τ
DAMM	*WD*	92.87%	16.23	0.98 (p = 0.34)	-0.08 (p = 0.66)
	MBD	97.78%	25.38	-0.24 (p = 0.81)	0.03 (p = 0.90)
	COMBINED	95.63%	20.62	0.12 (p = 0.90)	0.05 (p = 0.65)
Atwater	*WD*	85.75%	39.14	3.37 (p = 0.003)	0.19 (p = 0.31)
	MBD	91.84%	27.00	0.37 (p = 0.71)	0.03 (p = 0.90)
	COMBINED	88.52%	32.55	0.97 (p = 0.34)	0.13 (p = 0.27)

The improvement in COD_m predictions by the DAMM model, compared to the commonly used Atwater factors (15), demonstrates that the DAMM model is a promising alternative to the current Atwater approach. One of the primary advantages of using the DAMM model is that it provides added insight by distinguishing between the upper and lower gastrointestinal tracts and explicitly incorporating microbial metabolism. This contrasts to the traditional Atwater approach,

which treats the entire digestive system as a "black box." We show that the Atwater factors had a systematic bias of consistently underpredicting metabolizable COD_m, particularly for the WD. The source of the bias could be a *de facto* underestimation of SCFA absorption on diets that contain fewer complex carbohydrates. By explicitly including SCFA production and absorption, the DAMM model more accurately captured the microbial contribution.

Conclusion

Microorganisms play a fundamental role in human digestion and are essential for colonic health (59), but standard methods of calculating metabolizable energy (15) do not provide any insight into the composition and metabolic functioning of the colon's microbial community. The DAMM model overcomes this limitation, because it predicts the structure and function of the colon's microbial community for a specific diet. The DAMM model provides a mechanistic framework that divides the digestive tract into two major physiological sections and explicitly includes microbial metabolism. DAMM model predictions allow us to know if a diet is starving or adequately feeding the colon's microbial community.

By representing the structure and metabolic function of the colon's microbial community, the DAMM model 1) introduced an opportunity to develop human metabolic models that incorporate absorption of microbially produces SCFAs in the future; 2) captured observed differences between the two diets in terms microbially derived SCFAs, fecal COD, and in metabolizable COD; 3) pointed to methanogens accumulating in epithelial biofilms which tells us more about possible community structure and improved methane predictions; and 4) reduced systematic bias inherent in the Atwater model, which does not explicitly include the microbiome.

References

1. Krajmalnik-Brown R, Ilhan Z-E, Kang D-W, DiBaise JK. Effects of Gut Microbes on Nutrient Absorption and Energy Regulation. Nutr Clin Pract. 2012;27:201–14. Available from: http://doi.wiley.com/10.1177/0884533611436116
2. Oliphant K, Allen-Vercoe E. Macronutrient metabolism by the human gut microbiome: major fermentation by-products and their impact on host health. Microbiome 2019 71. BioMed Central; 2019;7:1–15. Available from: https://microbiomejournal.biomedcentral.com/articles/10.1186/s40168-019-0704-8
3. Wang B, Yao M, Lv L, Ling Z, Li L. The Human Microbiota in Health and Disease. Engineering. 2017;3:71–82. Available from: https://www.sciencedirect.com/science/article/pii/S2095809917301492
4. Romieu I, Dossus L, Barquera S, Blottière HM, Franks PW, Gunter M, Hwalla N, Hursting SD, Leitzmann M, Margetts B, et al. Energy balance and obesity: what are the main drivers? Cancer Causes Control. 2017;28:247–58.
5. Asnicar F, Berry SE, Valdes AM, Nguyen LH, Piccinno G, Drew DA, Leeming E, Gibson R, Le Roy C, Khatib H Al, et al. Microbiome connections with host metabolism and habitual diet from 1,098 deeply phenotyped individuals. Nat Med. Nature Research; 2021;27:321–32. Available from: https://doi.org/10.1038/s41591-020-01183-8
6. DiBaise JK, Zhang H, Crowell MD, Krajmalnik-Brown R, Decker GA, Rittmann BE. Gut Microbiota and Its Possible Relationship With Obesity. Mayo Clin Proc. 2008;83:460–9.
7. Kang D-W, Adams JB, Coleman DM, Pollard EL, Maldonado J, McDonough-Means S, Caporaso JG, Krajmalnik-Brown R. Long-term benefit of Microbiota Transfer Therapy on autism symptoms and gut microbiota. Sci Rep. 2019;9:5821. Available from:

http://www.ncbi.nlm.nih.gov/pubmed/30967657

8. Seira C, Robertson RC, Stanton C, Cryan JF, Dinan TG. Food for thought : The role of nutrition in the microbiota-gut e brain axis. Clin Nutr Exp. 2016;6:25–38. Available from: https://www.sciencedirect.com/science/article/pii/S235293931600004X

9. Singh RK, Chang HW, Yan D, Lee KM, Ucmak D, Wong K, Abrouk M, Farahnik B, Nakamura M, Zhu TH, et al. Influence of diet on the gut microbiome and implications for human health. J Transl Med. BioMed Central; 2017;1–17.

10. Elia M, Cummings JH. Physiological aspects of energy metabolism and gastrointestinal effects of carbohydrates. Eur J Clin Nutr. Nature Publishing Group; 2007;61:S40–74.

11. Rittmann BE, McCarty PL. Environmental biotechnology. Technology Guide: Principles and Applications. 2nd ed. McGraw-Hill Book Co; 2020.

12. Davis TL, Dirks B, Carnero EA, Corbin KD, Krakoff J, Parrington S, Lee D, Smith SR, Rittmann BE, Krajmalnik-Brown R, et al. Chemical Oxygen Demand can be Converted to Gross Energy for Food Items Using a Linear Regression Model. J Nutr. 2021;151:445–53.

13. US Department of Agriculture. Energy value of foods. Basic and derivation. Agric Handb no 74. 1973;2–11.

14. Kraisid Tontisirin., MacLean WC, Warwick P, Food and Agriculture Organization of the United Nations. Technical Workshop on Food Energy: Methods of Analysis and Conversion Factors [Internet]. Rome, Italy: Food and Agriculture Organization of the United Nations; 2003. Available from: http://www.fao.org/3/y5022e/y5022e00.htm#Contents

15. Atwater WO, Woods CD. The Chemical Composition of 162 American Food Materials. 1896.

16. Livesey G. The Energy Values of Dietary Fibre and Sugar Alcohols for Man. Nutr Res Rev. Cambridge University Press; 1992;5:61–84. Available from: https://www.cambridge.org/core/journals/nutrition-research-reviews/article/energy-values-of-dietary-fibre-and-sugar-alcohols-for-man/E3475A3F532E575C4E671D6F1E222913

17. Kettle H, Louis P, Holtrop G, Duncan SH, Flint HJ. Modelling the emergent dynamics and major metabolites of the human colonic microbiota. Environ Microbiol. 2015;17:1615–30.

18. Goodman AL, Kallstrom G, Faith JJ, Reyes A, Moore A, Dantas G, Gordon JI. Extensive personal human gut microbiota culture collections characterized and manipulated in gnotobiotic mice. PNAS. 2011;108:6252–7.

19. Cheng M, Ning K. Stereotypes About Enterotype: the Old and New Ideas. Genomics, Proteomics and Bioinformatics. Beijing Genomics Institute; 2019. p. 4–12.

20. Arumugam M, Raes J, Pelletier E, Le Paslier D, Yamada T, Mende DR, Fernandes GR, Tap J, Bruls T, Batto J-M, et al. Enterotypes of the human gut microbiome. Nature. 2011;473:174–80.

21. Xu Z, Knight R. Dietary effects on human gut microbiome diversity q. Br J Nutr. 2015;113:1–5. Available from: https://doi.org/10.1017/S0007114514004127

22. Corbin KD, Carnero EA, Dirks B, Igudesman D, Yi F, Marcus A, Davis TL, Pratley RE, Rittmann BE, Krajmalnik-Brown R, et al. Host-diet-gut microbiome interactions influence human energy balance: a randomized clinical trial. Nat Commun 2023 141. Nature Publishing Group; 2023;14:1–17. Available from: https://www.nature.com/articles/s41467-023-38778-x

23. Zou ML, Moughan PJ, Awati A, Livesey G. Accuracy of the Atwater factors and related food energy conversion factors with low-fat, high-fiber diets when energy intake is reduced

spontaneously. Am J Clin Nutr. 2007;86:1649–56. Available from: https://watermark-silverchair-com.ezproxy1.lib.asu.edu/znu01207001649.pdf?token=AQECAHi208BE49Ooan9kkhW_Ercy7Dm3ZL_9Cf3qfKAc485ysgAAAugwggLkBgkqhkiG9w0BBwagggLVMIIC0QIBADCCAsoGCSqGSIb3DQEHATAeBglghkgBZQMEAS4wEQQMj5PVymiwnAA5TOTfAgEQgIICmwvjaSe1bfG5aTP7hYG

24. Sánchez-Peña MJ, Márquez-Sandoval F, Ramírez-Anguiano AC, Velasco-Ramírez SF, Macedo-Ojeda G, González-Ortiz LJ. Calculating the metabolizable energy of macronutrients: a critical review of Atwater's results. Nutr Rev. Oxford Academic; 2017;75:37–48. Available from: https://academic.oup.com/nutritionreviews/article/75/1/37/2684502

25. Baer DJ, Gebauer SK, Novotny JA. Walnuts Consumed by Healthy Adults Provide Less Available Energy than Predicted by the Atwater Factors. J Nutr. 2016;146:9–13. Available from: http://jn.nutrition.org/cgi/doi/10.3945/jn.115.217372

26. Tulley RT, Appel MJ, Enos TG, Hegsted M, Mccutcheon KL, Zhou J, Raggio AM, Jeffcoat R, Birkett A, Martin RJ, et al. Comparative methodologies for measuring metabolizable energy of various types of resistant high amylose corn starch. J Agric Food Chem. 2009;57:8474–9.

27. Marcus A, Davis TL, Rittmann BE, DiBaise JK, Carnero EA, Corbin K, Smith SR, Krajmalnik-Brown R. Developing a model for estimating the activity of colonic microbes after intestinal surgeries. Carbonero F, editor. PLoS One. Public Library of Science; 2021;16:e0253542. Available from: https://journals.plos.org/plosone/article?id=10.1371/journal.pone.0253542

28. U.S. Department of Agriculture, Agricultural Research Service, Beltsville Human Nutrition Research Center. FoodData Central version 6.0 [Internet]. https://fdc.nal.usda.gov/. 2023. Available from: https://fdc.nal.usda.gov/

29. Corbin KD, Krajmalnik-Brown R, Carnero EA, Bock C, Emerson R, Rittmann BE, Marcus AK, Davis T, Dirks B, Ilhan ZE, et al. Integrative and quantitative bioenergetics: Design of a study to assess the impact of the gut microbiome on host energy balance. Contemp Clin Trials Commun. Elsevier; 2020;19:100646. Available from: https://linkinghub.elsevier.com/retrieve/pii/S2451865420301307

30. Wang YT, Mohammed SD, Farmer AD, Wang D, Zarate N, Hobson AR, Hellström PM, Semler JR, Kuo B, Rao SS, et al. Regional gastrointestinal transit and pH studied in 215 healthy volunteers using the wireless motility capsule: influence of age, gender, study country and testing protocol. Aliment Pharmacol Ther. John Wiley & Sons, Ltd; 2015;42:761–72. Available from: https://onlinelibrary.wiley.com/doi/full/10.1111/apt.13329

31. Dirks B, Davis TL, Carnero EA, Corbin KD, Smith SR, Rittmann BE, Krajmalnik-Brown R. Methanogens are associated with altered microbial production of short-chain fatty acids and human-host metabolizable energy. bioRxiv. Cold Spring Harbor Laboratory; 2025;2024.12.31.630929. Available from: https://www.biorxiv.org/content/10.1101/2024.12.31.630929v1

32. Djemai K, Drancourt M, Tidjani Alou M. Bacteria and Methanogens in the Human Microbiome: a Review of Syntrophic Interactions. Microb Ecol 2021 833. Springer; 2021;83:536–54. Available from: https://link.springer.com/article/10.1007/s00248-021-01796-7

33. Angelakis E, Armougom F, Million M, Raoult D. The relationship between gut microbiota and weight gain in humans. Future Microbiology. 2012. p. 91–109.

34. Balch WE, Fox GE, Magrum LJ, Woese CR, Wolfe RS. Methanogens: reevaluation of a unique biological group. Microbiol Rev. American Society for Microbiology (ASM); 1979;43:260. Available from: https://www.ncbi.nlm.nih.gov/pmc/articles/PMC281474/

35. Håvelsrud OE, Haverkamp THA, Kristensen T, Jakobsen KS, Rike AG. A metagenomic study of methanotrophic microorganisms in Coal Oil Point seep sediments. BMC Microbiol. BioMed Central Ltd.; 2011;11:1–14. Available from: https://bmcmicrobiol.biomedcentral.com/articles/10.1186/1471-2180-11-221

36. Stephen AM, Haddad AC, Phillips SF. Passage of carbohydrate into the colon. Direct measurements in humans. Gastroenterology. Elsevier Masson SAS; 1983;85:589–95. Available from: http://dx.doi.org/10.1016/0016-5085(83)90012-4

37. Ndou SP, Kiarie E, Walsh MC, Ames N, M de Lange CF, Nyachoti CM. Interactive effects of dietary fibre and lipid types modulate gastrointestinal flows and apparent digestibility of fatty acids in growing pigs. Br J Nutr. 2018;121:469–80. Available from: https://doi.org/10.1017/S0007114518003434

38. Rowan AM, Moughan PJ, Wilson MN, Maher K, Tasman-Jones C. Comparison of the ileal and faecal digestibility of dietary amino acids in adult humans and evaluation of the pig as a model animal for digestion studies in man. Br J Nutr. 1994;71:29–42.

39. Müller M, Canfora EE, Blaak EE. Gastrointestinal Transit Time, Glucose Homeostasis and Metabolic Health: Modulation by Dietary Fibers. Nutrients. Multidisciplinary Digital Publishing Institute (MDPI); 2018;10. Available from: /pmc/articles/PMC5872693/?report=abstract

40. Clegg M, Shafat A. Gastric emptying and orocaecal transit time of meals containing lactulose or inulin in men. 2020; Available from: https://doi.org/10.1017/S0007114510000905

41. Moorthy AS, Eberl HJ. Assessing the influence of reactor system design criteria on the performance of model colon fermentation units. 2013; Available from: http://dx.doi.org/10.1016/j.jbiosc.2013.09.015

42. Moorthy AS, Brooks SPJ, Kalmokoff M, Eberl HJ. A Spatially Continuous Model of Carbohydrate Digestion and Transport Processes in the Colon. PLoS One. Public Library of Science; 2015;10:e0145309. Available from: https://journals.plos.org/plosone/article?id=10.1371/journal.pone.0145309

43. Ramsay IR, Pullammanappallil PC. Protein degradation during anaerobic wastewater treatment : derivation of stoichiometry. Biodegradation. 2001;12:247–57.

44. Stolyar S, Van Dien S, Hillesland KL, Pinel N, Lie TJ, Leigh JA, Stahl DA. Metabolic modeling of a mutualistic microbial community. Mol Syst Biol. 2007;3:1–14.

45. Carnero E, Bock C, Liu Y, Corbin K, Wohlers-Kariesch E, Ruud K, Moon J, Marcus A, Rosa K-B, Muraviev A, et al. Measurement of 24-hour Continuous Human CH4 Release in a Whole Room Indirect Calorimeter [Internet]. Preprint. ResearchGate; 2022. Available from: https://www.researchgate.net/publication/365309180_Measurement_of_24-hour_Continuous_Human_CH4_Release_in_a_Whole_Room_Indirect_Calorimeter

46. Jones E, Oliphant T, Peterson P. SciPy: Open Source Scientific Tools for Python [Internet]. Available from: http://www.scipy.org/

47. Johnson LR. Gastrointestinal physiology - Chapter 11: Digestion and absorption of nutrients. 9th ed. Memphis: Elsevier; 2019. 102–120 p.

48. Boets E, Gomand S V., Deroover L, Preston T, Vermeulen K, De Preter V, Hamer HM, Van den Mooter G, De Vuyst L, Courtin CM, et al. Systemic availability and metabolism of colonic-derived short-chain fatty acids in healthy subjects: a stable isotope study. J Physiol. 2017;595:541–55.

49. Hall KD. Predicting metabolic adaptation, body weight change, and energy intake in humans. Am J Physiol Metab. 2009;298:E449–66.

50. Ruppin H, Bar-Meir S, Soergel KH, Wood CM, Schmitt MG. Absorption of short-chain fatty acids by the colon. Gastroenterology. Elsevier Masson SAS; 1980;78:1500–7. Available from: https://doi.org/10.1016/S0016-5085(19)30508-6

51. den Besten G, van Eunen K, Groen AK, Venema K, Reijngoud D-J, Bakker BM. The role of short-chain fatty acids in the interplay between diet, gut microbiota, and host energy metabolism. J Lipid Res. 2013;54:2325–40. Available from: http://www.jlr.org/lookup/doi/10.1194/jlr.R036012

52. Jensen MB, Strübing D, de Jonge N, Nielsen JL, Ottosen LDM, Koch K, Kofoed MVW. Stick or leave – Pushing methanogens to biofilm formation for ex situ biomethanation. Bioresour Technol. Elsevier; 2019;291:121784.

53. Bang C, Ehlers C, Orell A, Prasse D, Marlene S, Gorb SN, Albers SV, Schmitz RA. Biofilm formation of mucosa-associated methanoarchaeal strains. Front Microbiol. Frontiers Media S.A.; 2014;5:353. Available from: https://pmc.ncbi.nlm.nih.gov/articles/PMC4086402/

54. Samuel BS, Hansen EE, Manchester JK, Coutinho PM, Henrissat B, Fulton R, Latreille P, Kim K, Wilson RK, Gordon JI. Genomic and metabolic adaptations of Methanobrevibacter smithii to the human gut. Proc Natl Acad Sci U S A. Proc Natl Acad Sci U S A; 2007;104:10643–8. Available from: https://pubmed.ncbi.nlm.nih.gov/17563350/

55. Swidsinski A, Weber J, Loening-Baucke V, Hale LP, Lochs H. Spatial organization and composition of the mucosal flora in patients with inflammatory bowel disease. J Clin Microbiol. 2005;43:3380–9. Available from: https://journals.asm.org/journal/jcm

56. Macfarlane S, Dillon JF. Microbial biofilms in the human gastrointestinal tract. J Appl Microbiol. Blackwell Publishing Ltd; 2007;102:1187–96.

57. Samuel BS, Shaito A, Motoike T, Rey FE, Backhed F, Manchester JK, Hammer RE, Clay Williams S, Crowley J, Yanagisawa M, et al. Effects of the gut microbiota on host adiposity are modulated by the short-chain fatty-acid binding G protein-coupled receptor, Gpr41. 2008; Available from: www.pnas.org/cgi/content/full/

58. Armougom F, Henry M, Vialettes B, Raccah D, Raoult D. Monitoring Bacterial Community of Human Gut Microbiota Reveals an Increase in Lactobacillus in Obese Patients and Methanogens in Anorexic Patients. PLoS One. PLOS; 2009;4. Available from: /pmc/articles/PMC2742902/

59. Clemente JC, Ursell LK, Parfrey LW, Knight R. The impact of the gut microbiota on human health: An integrative view. Cell. 2012;148:1258–70.